Two-Dimensional Vortex Dynamics With Background Vorticity

David A. Schecter

Advanced Study Program
National Center for Atmospheric Research,[1] *P.O. Box 3000, Boulder, CO 80307*

Abstract. Magnetized electron plasmas have been used to study the dynamics of two-dimensional vortices in a cloud of background vorticity. Experiments have shown that background vorticity can calm chaotic vortex motion, and cool a system of intense vortices into a crystal equilibrium. Further experiments have shown that weak vortices tend to migrate to extrema in the background vorticity distribution. The electron plasma experiments have motivated new theories on two-dimensional vortex dynamics with background vorticity. The experiments and related theories are summarized.

Energetic, roughly two-dimensional (2D) vortices abound in nature [1]. Examples are oceanic eddies, tropical cyclones, and the Jovian hurricanes. Remarkably, magnetized electron plasmas are excellent systems for studying high Reynolds-number 2D vortex dynamics experimentally [2]. Recent electron plasma experiments have shed light on how 2D vortices interact with the environmental flow, i.e., with background vorticity. This article reviews the experiments, and related theories.

ELECTRON PLASMA EXPERIMENTS

Figure 1 is a schematic diagram of the experimental device [2]. A long column of electrons is confined in a hollow cylindrical conductor. The electrons are trapped axially by negative dc voltages on two end-cylinders, and radially by a uniform axial magnetic field $B\hat{z}$. The apparatus is equipped to destructively measure the z-averaged electron density $n(r, \theta, t)$. By raising the voltage of one end-cylinder (right), the electrons are released onto a phosphor screen. The resulting density image is recorded with a CCD camera. The evolution of n is observed by a sequence of experiments, in which the the initial conditions are the same, but the release-times vary.

Under proper conditions [2], the electron density n is governed approximately by a set of two-dimensional fluid equations, known as 2D drift-Poisson flow:

[1] The National Center for Atmospheric Research is supported by the National Science Foundation.

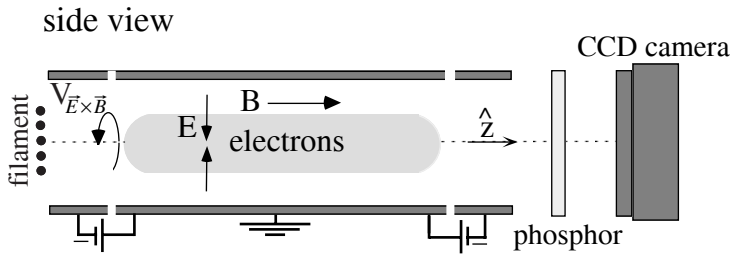

FIGURE 1. Confinement device (Penning-Malmberg trap) and imaging diagnostic, used to study 2D vortex dynamics with an electron plasma.

$$\frac{\partial n}{\partial t} + \vec{v} \cdot \nabla n = 0, \qquad \vec{v} = -\nabla \frac{c}{B}\phi \times \hat{z}, \qquad \nabla^2 \phi = 4\pi e n. \tag{1}$$

Here, $\vec{v}(r, \theta, t)$ is the $\vec{E} \times \vec{B}$ drift velocity field, and $\phi(r, \theta, t)$ is a 2D electrostatic potential. The boundary condition on the electrostatic potential is $\phi = 0$ at the wall of the confinement cylinder.

Defining the streamfunction, $\psi(r, \theta, t) \equiv c\phi/B$, and the vorticity, $\zeta(r, \theta, t) \equiv \hat{z} \cdot \nabla \times \vec{v}$, we may recast 2D drift-Poisson flow as follows:

$$\frac{\partial \zeta}{\partial t} + \vec{v} \cdot \nabla \zeta = 0, \qquad \vec{v} = -\nabla \psi \times \hat{z}, \qquad \nabla^2 \psi = \zeta. \tag{2}$$

By amazing coincidence, Eqs. (2) are the 2D Euler equations, which also govern two-dimensional flows in uniform-density inviscid incompressible fluids.

Comparing (2) to (1), we see that the vorticity ζ is proportional to the electron density n by the relation $\zeta = 4\pi e c B^{-1}\, n$. So, in the electron plasma experiments, *measuring electron density is equivalent to measuring vorticity.*

CHAOS TO CRYSTAL

Figure 2(a) shows the evolution of electron density (vorticity) in an experiment performed at the University of California, San Diego [3]. Initially, the density is distributed in a spiral, resembling a hot tungsten filament that is used to create the electrons. Subsequently, the density evolves into a system of N clumps (dark spots) immersed in a diffuse background plasma. Each density clump corresponds to an intense vortex, spinning counter-clockwise, and the diffuse background plasma corresponds to a low level of background vorticity.

To appreciate the influence of background vorticity on the vortex motion, let us first consider the vortex dynamics without background vorticity. In the absence of background vorticity, the vortex dynamics is Hamiltonian. Ignoring minor wall effects, the Hamiltonian is given by [4]

$$H = -\frac{1}{4\pi} \sum_{i<j} \Gamma_i \Gamma_j \, ln \left[(x_i - x_j)^2 + (y_i - y_j)^2 \right], \tag{3}$$

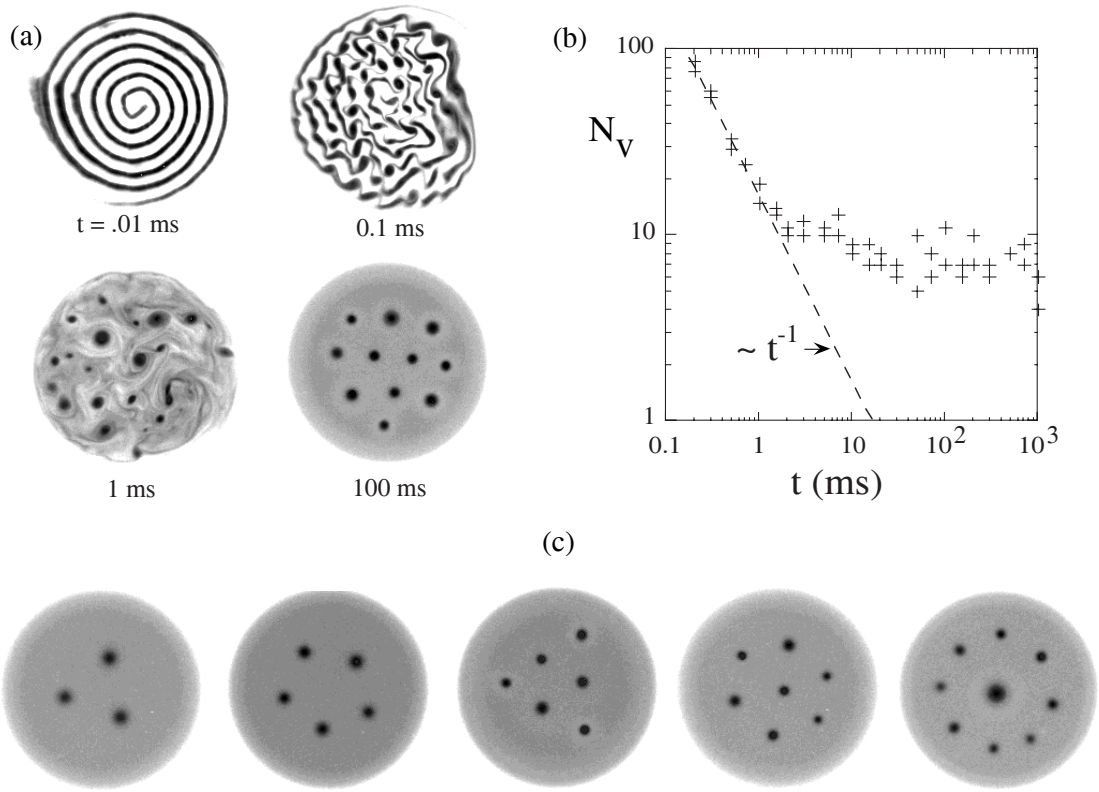

FIGURE 2. Spontaneous formation of a vortex crystal in an initially turbulent electron plasma [3]. (a) Time evolution of z-averaged electron density (vorticity). Darker shades indicate higher density. (b) Number of vortices versus time. (c) Selection of vortex crystals obtained from initial conditions similar to that in (a).

where Γ_i is the circulation (area integral of vorticity) of the i^{th} vortex, (x_i, y_i) is the position of the i^{th} vortex in a Cartesian coordinate system, and $i, j = 1, 2, \ldots N$. The canonically conjugate coordinates are $(q_i, p_i) \equiv (\sqrt{\Gamma_i}\ x_i,\ \sqrt{\Gamma_i}\ y_i)$, and the dynamics is given by Hamilton's equations: $\dot{q}_i = \partial_{p_i} H$, $\dot{p}_i = -\partial_{q_i} H$.

Because the vortex dynamics is Hamiltonian (without background vorticity), it is generally chaotic. During this chaotic motion, two vortices occasionally become close enough to merge. Numerical simulations of 2D Hamiltonian vortex dynamics, punctuated by occasional mergers, show that the number of vortices N_v decays as a power law in time, $t^{-\xi}$, where ξ is a positive constant of order unity [5]. Figure 2(b) compares the expected power-law decay to an electron plasma experiment. The scatter in the data is due to the destructive imaging technique. Initially, N_v exhibits the expected power-law decay; however, when $t \simeq 10$ms, mergers cease.

The arrest of vortex mergers is due to the formation of a "vortex crystal" equilibrium [Fig 2(a), 100ms; Fig. 2(c)]. A vortex crystal is an array of intense vortices that rotates rigidly in a diffuse background. Jin and Dubin proposed that vortex crystals form due to the ergodic mixing of background vorticity by the intense vor-

tices [6]. Using a version of Lynden-Bell statistics [7], they showed that a vortex crystal equilibrium is the most probable state that can result from such mixing, for a given energy, angular momentum and total circulation of the flow. These maximum entropy states are compared to the experiments in Ref. [6]: they accurately predict the arrangement of vortices, and details of the background vorticity distribution.[2] Since the electron plasma experiments, the formation of vortex crystals has been observed in various numerical simulations of 2D Euler flow [8,9].

MOTION TO THE EXTREMA

The spontaneous formation of vortex crystals in 2D turbulence demonstrates the importance of background vorticity in spectacular fashion. Of course, other effects of background vorticity have been recognized for decades. For example, it is well-known that vortices move toward extrema of the background vorticity distribution. The details of this process have been studied rigorously in dynamical meteorology [12], for the main purpose of understanding hurricane trajectories.[3] However, a new theory was required to explain the vortex motion in electron plasmas [13].

Unlike terrestrial hurricanes, vortices in electron plasmas are typically exposed to intense background shear. In this sense, electron vortices are more like Jovian hurricanes, which are contained in strongly sheared zonal jets [10], or mesovortices within hurricanes [9,11]. Intense background shear creates a disparity in the rates at which vortices of opposite sign migrate to extrema of background vorticity. Furthermore, sufficiently large shear will arrest the migration. These results are discussed below.

Figure 3(a) is a numerical simulation that illustrates vortex motion through axisymmetric background vorticity, similar to what might exist in an electron plasma. At $t = 0$, a clump (black dot) and a hole (white dot) are placed at the same radius r_v. The clump is a positive vortex, spinning counter-clockwise, whereas the hole is a negative vortex, spinning clockwise. In time, both vortices redistribute the local background vorticity. In response, the clump moves radially inward, to the peak of background vorticity, whereas the hole moves radially outward, toward a minimum of background vorticity.

The opposite motion of clumps and holes is easily understood. Suppose that there is only one vortex of circulation Γ_v, and that the vortex is point-like. The vorticity distribution is a sum of the background contribution (b) and the vortex contribution (v); i.e., $\zeta = \zeta_b + \Gamma_v \delta(\vec{r} - \vec{r}_v)$. It is well-known that the 2D Euler equations, with rotationally symmetric boundary conditions, conserve the canonical angular momentum,

---

[2] The final number of vortices and their individual vorticity profiles are not predicted. They are taken from the observed vortex crystals and fixed in computing the maximum entropy states.

[3] The background vorticity affecting hurricane motion includes planetary vorticity, as well as the vorticity associated with the environmental wind.

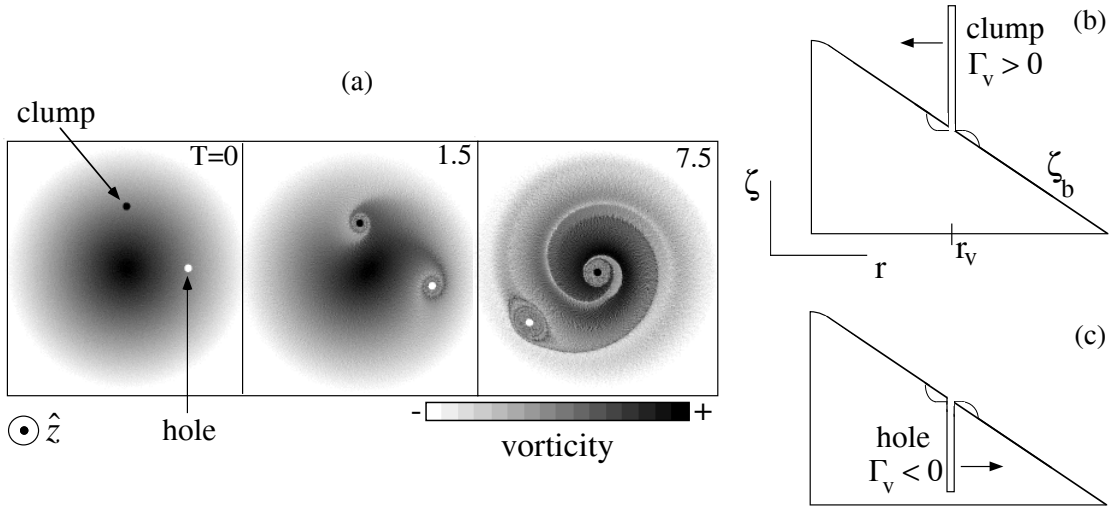

FIGURE 3. Vortex motion in an axisymmetric background vorticity distribution. (a) Numerical simulation. $T \equiv t \times |S[r_v(0)]|$. (b,c) The redistribution of local background vorticity by a vortex increases $< r^2 >_b$. By conservation of P_θ, clumps and holes must react oppositely.

$$P_\theta \equiv \int d^2\vec{r}\,\zeta r^2 = \Gamma_b < r^2 >_b + \Gamma_v\, r_v^2. \tag{4}$$

Here, $\Gamma_b > 0$ is the total circulation of the background flow, and $< r^2 >_b$ is the ζ_b-weighted spatial average of r^2. As illustrated in Figs. 3(b) and 3(c), the redistribution of background vorticity by the vortex tends to create a local plateau in the θ-average of ζ_b. This increases $< r^2 >_b$. To conserve P_θ, a clump ($\Gamma_v > 0$) must decrease r_v and move up the background vorticity gradient, whereas a hole ($\Gamma_v < 0$) must increase r_v and move down the gradient.

Let us now consider the vortex-background interaction in greater detail. The Euler equation for the evolution of vorticity can be written as two separate equations. The first equation is for the vortex motion,

$$\frac{d}{dt}\vec{r}_v = \vec{v}_b(r_v, \theta_v, t). \tag{5}$$

Here, $\vec{v}_b$ is the background velocity field; that is, $\vec{v}_b = -\nabla\psi_b \times \hat{z}$, where $\nabla^2\psi_b = \zeta_b$. Since the background vorticity is initially axisymmetric, i.e., $\zeta_b(\vec{r}, t = 0) = \bar{\zeta}_b(r)$, the background velocity is initially circular, i.e., $\vec{v}_b(\vec{r}, t = 0) = \bar{v}_b(r)\hat{\theta}$. The second equation is for the advection of background vorticity,

$$\frac{\partial}{\partial t}\zeta_b + (\vec{v}_b + \vec{v}_v) \cdot \nabla\zeta_b = 0, \tag{6}$$

where $\vec{v}_v = \hat{z} \times \Gamma_v(2\pi)^{-1}\nabla \ln(|\vec{r} - \vec{r}_v|)$ plus a small correction due to the wall. The vortex trajectory is obtained by integrating Eqs. (5) and (6) simultaneously.

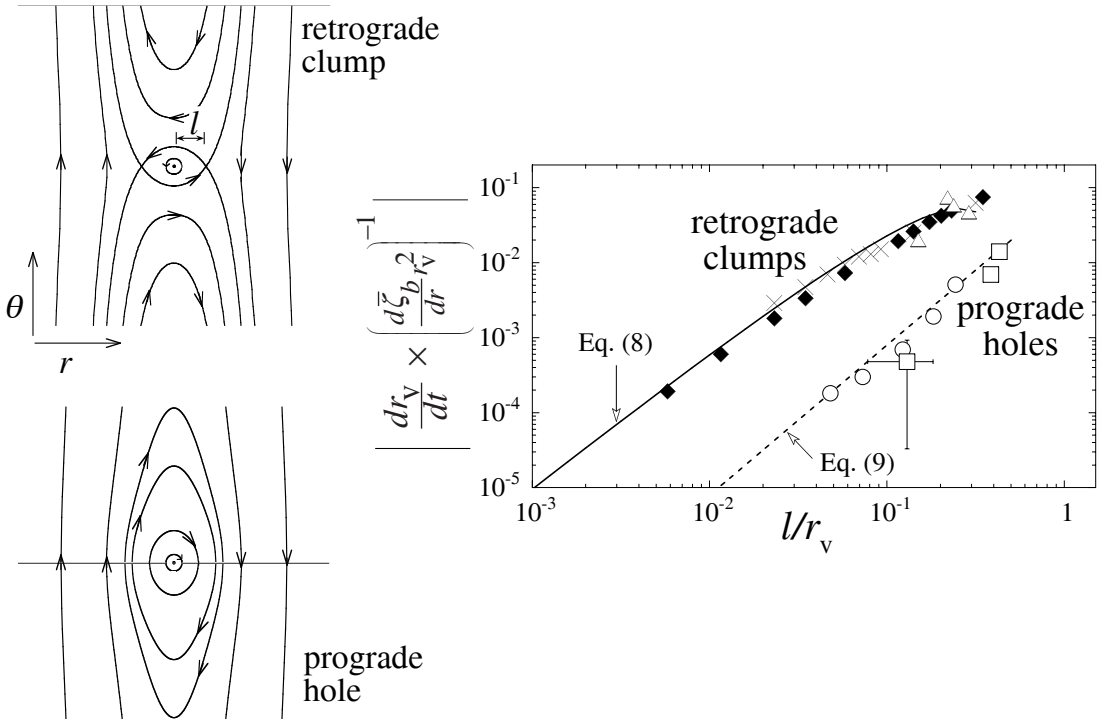

FIGURE 4. (Left) Stream lines about a retrograde clump and a prograde hole. (Right) The radial speeds of retrograde clumps and prograde holes of various strengths (l/r_v) in axisymmetric background vorticity. Retrograde clumps: the $\times$s and diamonds are numerical simulations, the triangles are electron plasma experiments, and Eq. (8) is computed with $c = 0.43$. Prograde holes: the circles are numerical simulations, and the squares are electron plasma experiments.

Neglecting changes to ζ_b [Eq. (6)], a single vortex merely orbits the center of background vorticity, with angular frequency $d\theta_v/dt = r_v^{-1}\bar{v}_b(r_v)$. However, as explained previously, the background vorticity perturbation causes the vortex to drift radially. The radial velocity, dr_v/dt, is sensitive to whether the vortex is retrograde or prograde. A vortex is retrograde if it rotates against the local background shear, whereas a vortex is prograde if it rotates with the local background shear. Precisely, let $S(r)$ denote the local shear-rate, $r\ d(\bar{v}_b r^{-1})/dr$. Then, $\Gamma_v/S(r_v) < 0$ for a retrograde vortex, whereas $\Gamma_v/S(r_v) > 0$ for a prograde vortex. Here, we consider examples in which the background vorticity decreases monotonically with r, so that $S(r)$ is negative. Therefore, in these examples, clumps are retrograde and holes are prograde.

The stream lines about a retrograde clump and a prograde hole are shown in Fig. 4 (left). There are two stagnation points at radial distances $\pm l$ from the center of the retrograde vortex, where

$$l \equiv \sqrt{\left|\frac{\Gamma_v}{2\pi S(r_v)}\right|}. \tag{7}$$

In contrast, there are no stagnation points in the vicinity of a prograde vortex.

Schecter and Dubin [13] derived analytical expressions for the radial velocities of retrograde and prograde vortices, for the regime in which $l/r_v << 1$. This regime corresponds to a weak vortex in strong background shear. For a retrograde vortex,

$$\frac{d}{dt}r_v \;=\; \pm\,\frac{\pi}{2}\,\frac{d\bar{\zeta}_b}{dr}(r_v)\;l^2\;ln\,(c\;r_v/l)\,, \tag{8}$$

where $+/-$ is for clumps/holes, and c is a constant of order unity that depends on the particular form of $\bar{\zeta}_b(r)$. For a prograde vortex,

$$\frac{d}{dt}r_v \;=\; \pm\,\frac{1}{4\pi}\,\frac{d\bar{\zeta}_b}{dr}(r_v)\;l^2. \tag{9}$$

In both cases, the radial speed increases with the local background vorticity gradient, and decreases as the local shear-rate intensifies. Note that the prefactor $(1/4\pi)$ in Eq. (9) is much less than the prefactor $(\pi/2)$ in Eq. (8). Moreover, the logarithmic factor does not appear in Eq. (9). Thus, as l/r_v approaches zero, a prograde vortex will move orders of magnitude slower than a retrograde vortex of equal strength.

The plot in Fig. 4 shows the radial vortex velocity (dr_v/dt) as a function of vortex strength (l/r_v) for a set of numerical simulations, and for several electron plasma experiments. In each case, a single vortex moved through a background vorticity resembling that in Fig. 3(a).[4] The simulations are described in Ref. [13], and the experiments are described in Refs. [14,15]. The data compares favorably to the analytical predictions of Schecter and Dubin. Recently, Kiwamoto and collaborators used a magnetized electron plasma to examine the motion of retrograde clumps more extensively [16]. Their data also agrees with Eq. (8).

The data in Fig. 4 are for cases in which $\varepsilon(r) \equiv \dfrac{d}{dr}\left(\dfrac{\bar{v}_b}{r}\right)\Big/\dfrac{d\bar{\zeta}_b}{dr} << 1$ at the radial position r_v of the vortex. However, if $\varepsilon(r_v)$ surpasses a critical value, Eqs. (8) and (9) become invalid, and the radial velocity of the vortex drops abruptly to zero. For prograde vortices, Schecter and Dubin estimated that the critical value of $\varepsilon(r_v)$ is unity. For retrograde vortices, Schecter and Dubin estimated that the critical value of $\varepsilon(r_v)$ is of order $\sqrt{8}\pi^2\sqrt{ln(r_v/l)}$. Both estimates are consistent with numerical simulations [13].

DANCING WITH THE DIOCOTRON MODES

The theoretical work of Schecter and Dubin [13] neglects the interaction of the vortex with the global modes of the background vorticity, i.e., the diocotron modes. While usually valid (Fig. 4), such neglect is unjustified if the orbital frequency of a vortex resonates with a neutral, or weakly damped diocotron mode. In such a case,

[4] There is one exception: the datum with error bars was obtained from an electron plasma experiment in which there were two prograde holes [15].

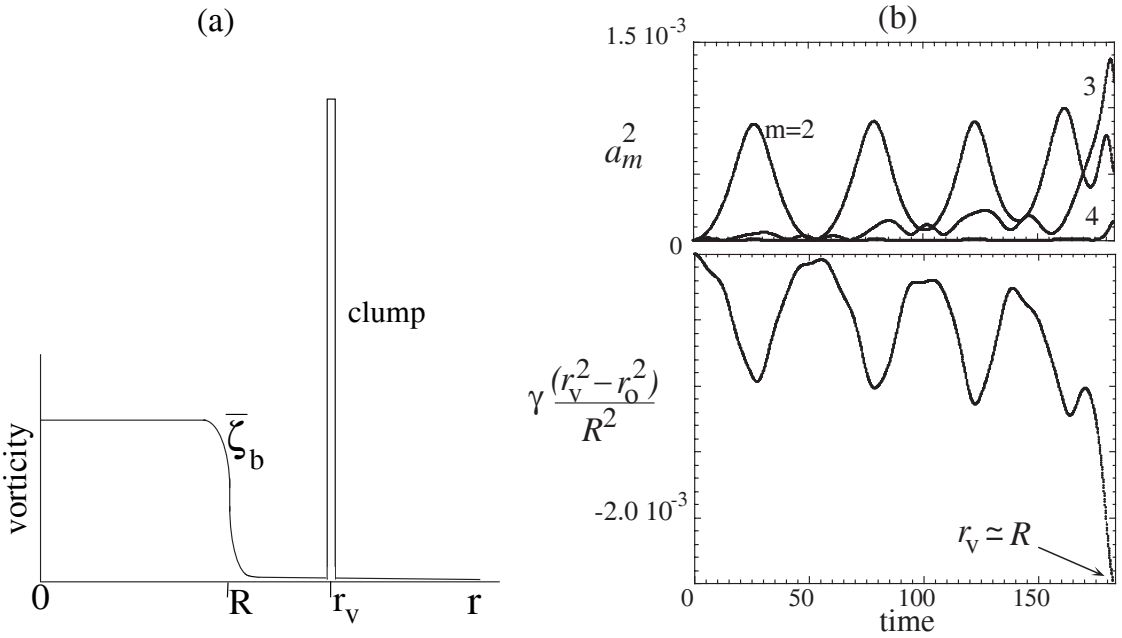

FIGURE 5. Example in which the radial motion of a clump is controlled by diocotron modes, as opposed to a local background vorticity perturbation. (a) Initial vorticity distribution. (b) Diocotron mode amplitudes and radial position of the clump versus time, in units of $2\pi R^2/\Gamma_b$. A sequence of resonances causes the clump to merge with the core of the background vorticity [17].

there can be significant radial motion even if $\dfrac{d\bar{\zeta}_b}{dr}(r_v)$ is zero, or if $\varepsilon(r_v)$ is above its critical value. The following example illustrates this point.

Consider the initial vorticity distribution in Fig. 5(a). The background vorticity $\bar{\zeta}_b(r)$ consists of a uniform core ($r < R$), and an outer skirt ($r > R$), where the vortex resides. By assumption, the vorticity in the outer skirt is negligible, so that $\Gamma_b \simeq \pi R^2 \bar{\zeta}_b(0)$. In addition, $d\bar{\zeta}_b/dr \simeq -\bar{\zeta}_b(0)\delta(r-R)$.

The background vorticity perturbation will be concentrated at the core radius R. Expanding this perturbation in a Fourier series yields

$$\zeta_b \;\simeq\; \bar{\zeta}_b(r) \;+\; \frac{\Gamma_b}{\pi R}\delta(r-R)\;\sum_{m=1}^{\infty} a_m(t)\;\cos[m\theta - \varphi_m(t)], \tag{10}$$

where $\Gamma_b/\pi R$ is a convenient normalization factor. The Fourier components are the "diocotron modes" of the background vorticity. Exciting a diocotron mode corresponds to displacing ($m = 1$) or deforming ($m \geq 2$) the core. In the following, it will be assumed that the vortex is weak and that the mode amplitudes are small; i.e., $\gamma \equiv \Gamma_v/\Gamma_b << 1$, and $a_m << 1$. Changes to the axisymmetric component of background vorticity are of order a_m^2, and are neglected in Eq. (10).

The vortex-mode dynamics may be put in Hamiltonian form [17]. The canonically conjugate variables for the m^{th} mode are $(q_m,\ p_m) \;\equiv\; (-\varphi_m,\ a_m^2/m)$, and the

canonically conjugate variables for the vortex are $(q_v,\ p_v) \equiv (-\sqrt{\gamma}\,\theta_v,\ \sqrt{\gamma}\,r_v^2/R^2)$. The equations of motion are Hamilton's equations: $(\dot{q}_m,\ \dot{p}_m) = (\partial_{p_m}H,\ -\partial_{q_m}H)$, and $(\dot{q}_v,\ \dot{p}_v) = (\partial_{p_v}H,\ -\partial_{q_v}H)$, where (ignoring wall effects)

$$H = -\frac{\Gamma_b}{2\pi R^2}\times \left\{\gamma\, ln(p_v) + \sum_{m=1}^{\infty}(m-1)\,p_m - 2\,\gamma\,\sum_{m=1}^{\infty}\gamma^{\frac{m}{4}}\sqrt{\frac{p_m}{mp_v^m}}\,\cos\left[\frac{m}{\sqrt{\gamma}}q_v - q_m\right]\right\}. \tag{11}$$

The first term in braces accounts for the advection of the vortex in the unperturbed circular flow. The middle term accounts for the free propagation of diocotron modes, in the absence of the vortex. The final term couples the vortex motion to the modes. The Hamiltonian in Eq. (11) neglects mode-mode interaction terms, which are of order a_m^2.

Of course, the vortex-mode interaction conserves canonical angular momentum. Minus the constant unperturbed background contribution, the (dimensionless) canonical angular momentum can be written as follows:

$$\tilde{P}_\theta = \sum_{m=1}^{\infty} a_m^2 + \gamma\frac{r_v^2}{R^2}. \tag{12}$$

Suppose that a clump ($\gamma > 0$) excites a mode. Then, $\sum a_m^2$ increases. To conserve $\tilde{P}_\theta$, r_v must decrease. In contrast, if a hole ($\gamma < 0$) excites a mode, r_v must increase to conserve $\tilde{P}_\theta$.

Figure 5(b) illustrates the vortex-mode dynamics governed by the Hamiltonian in Eq. (11). At $t = 0$, a clump ($\gamma = .0025$) is placed at $r_v = r_o = 1.418R$, and the mode amplitudes are all zero. The clump principally orbits the center of the background with angular velocity $d\theta_v/dt \simeq \bar{v}_b(r_v)/r_v = \Gamma_b/2\pi r_v^2$. At $r_v = 1.418R$, this angular velocity equals the natural phase velocity of the $m = 2$ diocotron mode. Consequently, the clump resonantly excites the $m = 2$ mode. By conservation of $\tilde{P}_\theta$, this resonance causes the clump to move radially inward. As the clump approaches the core, $d\theta_v/dt$ increases. This causes resonances with higher order diocotron modes: first the $m = 3$, then the $m = 4$, etc. The sequence of resonances incrementally pulls the clump into the core.

Lansky, O'Neil and Schecter [17] derived a condition for which the clump will merge with the core. For the case in which the initial clump position is $r_o = 1.418R$, γ must be greater than about 0.002. Otherwise, the initial oscillations of r_v [Fig. 5(b)] will not bring the clump close enough to the core to resonantly excite higher order modes. Electron plasma experiments have yet to verify this merger condition.

However, Durkin and Fajans [18] have used a magnetized electron plasma to examine the interaction of diocotron modes with a clump that is already inside the core ($r_v < R$). In this case, there are no vortex-mode resonances. Nevertheless, the clump can weakly excite the diocotron modes. This creates a wave along the

edge of the core. Eventually, the wave breaks. The wave-breaking process alters the background vorticity profile, and can generate one or more vorticity holes. The measured wave-breaking time is proportional to $\gamma^{-1}\ln(\gamma^{-1})$, provided that $r_v \lesssim 0.7R$. This result agrees with a recent theory by Jin and Dubin [19].

Clearly, background vorticity enriches 2D vortex dynamics. Background vorticity can cause the spontaneous formation of vortex crystals (Fig. 2), and can spatially separate vortices of opposite sign (Fig. 3). Recent work in non-neutral plasma physics has shed some light on 2D vortex dynamics with background vorticity, but surely more surprises await.

ACKNOWLEDGMENTS: The author thanks Prof. C.F. Driscoll and Dr. A. Kabantsev for providing experimental data. The author also thanks Prof. D.H.E. Dubin, Prof. T.M. O'Neil, Dr. I.M. Lanski and Dr. D.Z. Jin for their contributions to the theory presented. This research was supported in part by the National Science Foundation (PHY-9876999) and the Office of Naval Research (N00014-96-1-0239).

REFERENCES

1. D.G. Dritschel and B. Legras, Phys. Today **46**, 44 (1993).
2. C.F. Driscoll and K.S. Fine, Phys. Fluids B **2**, 1359 (1990).
3. K.S. Fine, A.C. Cass, W.G. Flynn and C.F. Driscoll, Phys. Rev. Lett. **75**, 3277 (1995).
4. G.K. Batchelor, *An Introduction to Fluid Dynamics*, Cambridge Univ. Press (1967).
5. G.F. Carnevale, J.C. McWilliams, Y. Pomeau, J.B. Weiss and W.R. Wang, Phys. Rev. Lett. **66**, 2735 (1991).
6. D.Z. Jin and D.H.E. Dubin, Phys. Rev. Lett. **80**, 4434 (1998).
7. D. Lynden-Bell, Mon. Not. R. Astron. Soc. **136**, 101 (1967).
8. D.A. Schecter, D.H.E. Dubin, K.S. Fine and C.F. Driscoll, Phys. Fluids **11**, 905 (1999); D.Z. Jin and D.H.E. Dubin, Phys. Rev. Lett. **84**, 1443 (2000).
9. J.P. Kossin and W.H. Schubert, J. Atmos. Sci. **58**, 2196 (2001).
10. R. Beebe, Chaos **4**, 113 (1994).
11. M.T. Montgomery, V.A. Vladimirov and P.V. Denissenko, J. Fluid Mech., submitted.
12. G.F. Carnevale, R.C Kloosterziel and G.J.F. Van Heist, J. Fluid Mech. **233**, 119 (1991); R.K. Smith and W. Ulrich, Q.J.R. Meteorol. Soc. **119**, 207 (1993); R.T. Williams and J. C.-L. Chan, J. Atmos. Sci. **51**, 1065 (1994); More in Ref. [13].
13. D.A. Schecter and D.H.E. Dubin, Phys. Rev. Lett. **83**, 2191 (1999); D.A. Schecter and D.H.E. Dubin, Phys. Fluids **13**, 1704 (2001).
14. A. Kabantsev, C.F. Driscoll, D.H.E. Dubin and D.A. Schecter, to appear in 11th Intl. Toki Conf. on Potential and Structure in Plasmas (Nagoya, Dec. 2000);
15. X.P. Huang, K.S. Fine and C.F. Driscoll, Phys. Rev. Lett. **74**, 4424 (1995).
16. Y. Kiwamoto, K. Ito, A. Sanpei and A. Mohri, Phys. Rev. Lett. **85**, 3173 (2000).
17. I.M. Lansky, T.M. O'Neil and D.A. Schecter, Phys. Rev. Lett. **79**, 1479 (1997).
18. D. Durkin and J. Fajans, Phys. Rev. Lett. **85**, 4052 (2000).
19. D.Z. Jin and D.H.E. Dubin, Phys. Fluids **13**, 677 (2001).